Journal of Applied Physics

Effect of fluorine on the suppression of boron diffusion in pre-amorphized silicon

Cite as: J. Appl. Phys. **128**, 105701 (2020); https://doi.org/10.1063/5.0015405
Submitted: 27 May 2020 . Accepted: 19 August 2020 . Published Online: 08 September 2020

Ryotaro Kiga, Masashi Uematsu, and Kohei M. Itoh

View Online

Export Citation

CrossMark

ARTICLES YOU MAY BE INTERESTED IN

Oxidation-enhanced Si self-diffusion in isotopically modulated silicon nanopillars
Journal of Applied Physics **127**, 045704 (2020); https://doi.org/10.1063/1.5134105

Effect of reactant dosing on selectivity during area-selective deposition of TiO_2 via integrated atomic layer deposition and atomic layer etching
Journal of Applied Physics **128**, 105302 (2020); https://doi.org/10.1063/5.0013552

Observation of carrier lifetime distribution in 4H-SiC thick epilayers using microscopic time-resolved free carrier absorption system
Journal of Applied Physics **128**, 105702 (2020); https://doi.org/10.1063/5.0015199

© 2020 Author(s).

Journal of Applied Physics ARTICLE scitation.org/journal/jap

Effect of fluorine on the suppression of boron diffusion in pre-amorphized silicon

Cite as: J. Appl. Phys. **128**, 105701 (2020); doi: 10.1063/5.0015405
Submitted: 27 May 2020 · Accepted: 19 August 2020 ·
Published Online: 8 September 2020

View Online Export Citation CrossMark

Ryotaro Kiga, Masashi Uematsu, and Kohei M. Itoh

AFFILIATIONS

School of Fundamental Science and Technology, Keio University, Yokohama 223-8522, Japan

[a)] **Author to whom correspondence should be addressed:** kitoh@appi.keio.ac.jp

ABSTRACT

The effect of fluorine (F) on diffusion of boron (B) in silicon (Si) is investigated by secondary ion mass spectrometry of Si, B, and F diffusion using pre-amorphized $^{nat}Si/^{28}Si$ isotope multilayers that are co-implanted with B and F. By the presence of F, diffusion of B is suppressed while that of Si is enhanced. A quantitative analysis of the experimental results based on our diffusion model shows that the suppression of B diffusion is due to (1) Si interstitial undersaturation caused by the time-dependent formation and dissolution of F-vacancy (FV) clusters and (2) direct interaction between B and FV clusters. The model developed in this study enables an accurate simulation of B and Si diffusion in the presence of F in Si.

Published under license by AIP Publishing. https://doi.org/10.1063/5.0015405

I. INTRODUCTION

Boron (B) implantation and post-annealing processes are widely used for the formation of p-type shallow junctions in silicon (Si) electronic devices, and the suppression of the transient enhanced diffusion (TED) of B is a crucial issue for continuous scaling down of device processing. Fluorine (F) has been reported to suppress the TED of B, and, therefore, co-doping of F is a promising method for the formation of ultra-shallow junctions.[1–13] Boron fluoride (BF_2) is an important implantation species not only because it includes both B and F but also because it has the smaller projected range than atomic B and is able to induce amorphization of Si.[1,3,4,6,7] The advantage of amorphization is that dopant channeling is reduced and that the damage in the amorphized region is almost totally eliminated through solid-phase epitaxial regrowth during post-implant annealing. During the regrowth, however, end-of-range (EOR) defects are formed, which are interstitial-type dislocation loops and become a source of TED. For these reasons, the effect of F on B diffusion in pre-amorphized Si has been studied extensively.[1,4,5,7,8,10,12]

Several works demonstrated that the presence of F reduced the supersaturation of self-interstitials (I's) that led to TED of B.[1,4,8–13] The experimental results suggested that the reduction of I concentration was caused by dissolution of F-vacancy (FV) clusters.[9–13] The presence of FV clusters in F-doped Si was predicted by theoretical calculations[14–15] and confirmed experimentally by positron annihilation spectroscopy[16–18] and electron paramagnetic resonance[19] of F-implanted Si. Another set of experiments argued that the suppression of B diffusion was caused mainly by direct chemical interaction between B and F.[2,3,7] The experiment using a buried B layer suggested that there was little direct interaction between F and I but there was a F–B interaction causing suppression of B diffusion.[7] The experiments conducted to probe the effect of F on the depth-dependent behaviors of point defects (I and V) using B delta-doped multilayers were not able to separate conclusively the effects between the FV clusters and F–B interaction.[5,13] Quantitative understanding of such competing mechanisms leading to the establishment of a model that can be implemented in technology computer-aided design (TCAD) semiconductor process simulators[20–22] is important.

The present work shows conclusively that the effects of FV clusters and F–B interaction co-exist. A unified model has been developed to describe experimental results quantitatively. Our experiments using silicon isotope multilayers are designed not only to show the importance of the two mechanisms but also to extract important parameters in the model to provide solid understanding of the physics behind the suppression of B diffusion by F. We simultaneously observe Si self-, B, and F diffusion using pre-amorphized Si isotope multilayers that are co-implanted with B and F. Using the Si isotope multilayers, the effect of F on the behaviors of point defects can be investigated via direct observation of Si self-diffusion[23–25] and so can be the effect of EOR defects on

point defects.[26,27] Implantation of F instead of BF_2 allows for observation of the effect of isolated F. We show that, by the presence of F, Si self-diffusion is enhanced, while B diffusion is suppressed, indicating the increase of V concentration. The shape and the time-dependent behavior of F profiles suggest the contribution of FV clusters, where the increase of V concentration is attributable to V emission upon the cluster dissolution. Moreover, B atoms at the F peak region are almost immobile, and the decrease of F concentration is suppressed only around the B high concentration region, suggesting a direct interaction between B and F, which suppresses B diffusion and the dissolution of FV clusters. Therefore, the suppression of B diffusion by the presence of F is attributed to both the I undersaturation caused by FV clusters and the direct F–B interaction. From these results, unlike the previous model that took only FV clusters into account,[20–22] we develop a model that takes both FV clusters and F–B interaction into account and achieve quantitative agreement with experimental results. For FV clusters, F_3V and F_6V_2 with a configuration change from F_3V to F_6V_2 are considered in order to model the reduction of dissolution rates with annealing time. In addition, the characteristic concentration, above which the dissolution rate of FV clusters decreases with the concentration, is introduced to reproduce the distinctive F profiles. For F–B interaction, the suppression of B diffusivities with higher concentration of FV clusters and that of the dissolution rates of FV clusters with higher B concentration are introduced.

It is demonstrated that the diffusion calculation based on these models agrees with the experimental profiles taken with various samples and under different annealing conditions. The calculations reproduce the time-dependent changes of the characteristic F profiles and immobile B profiles in the F peak region. Our model can be implemented in TCAD simulators for the process simulation of the ultra-shallow source–drain formation by co-implantation of B and F.

II. EXPERIMENTS

Isotopically enriched ^{28}Si and natural Si (92.2% ^{28}Si, 4.7% ^{29}Si, and 3.1% ^{30}Si) multilayers were grown by molecular beam epitaxy on a (100)-oriented Si wafer.[28] The multilayers consisted of nine periods of pairs of a 17 nm-thick ^{nat}Si and a 28 nm-thick ^{28}Si layer. The ^{nat}Si layers had the natural abundance with 3.1% of ^{30}Si, whereas ^{28}Si layers were depleted of ^{30}Si. Si self-diffusion was evaluated by observing the change of the ^{30}Si depth profiles after annealing. The Si isotope multilayers were first amorphized by $^{74}Ge^+$ ion implantation with an energy of 150 keV and a dose of 2×10^{15} cm^{-2}. Due to the implantation, amorphization occurred between the surface and 175 nm in depth, while the deeper region ($x > 175$ nm) remained single crystalline, as was shown in Fig. 2(a) of our previous study for the same implantation conditions.[26] After pre-amorphization, $^{19}F^+$ and/or $^{11}B^+$ were implanted, respectively, with 25 keV and 1×10^{15} cm^{-2}, and with 15 keV and 1×10^{14} cm^{-2}. The implantation energies of F and B were selected such that the peak of the F profile situated close to that of B and that the two profiles stayed within the pre-amorphized region. All the implantations were performed at room temperature. Four types of samples were prepared in this study; F and B implantation (F + B sample), F only (F), B only (B), and no F or B (control). The samples were annealed at 800–950 °C for 30 s–2 h in a rapid-thermal annealer or a resistive furnace under the continuous flow of pure Ar gas (99.99%) without prior deposition of a capping layer. The process flow is schematically shown in Fig. 1. The depth profiles of ^{30}Si, ^{11}B, ^{19}F, and ^{74}Ge were measured by secondary ion mass spectrometry (SIMS). Primary ions used in SIMS were O^{2+} with an energy of 1.0 keV for ^{30}Si and ^{11}B, and Cs^+ with 3.0 keV for ^{19}F and ^{74}Ge.

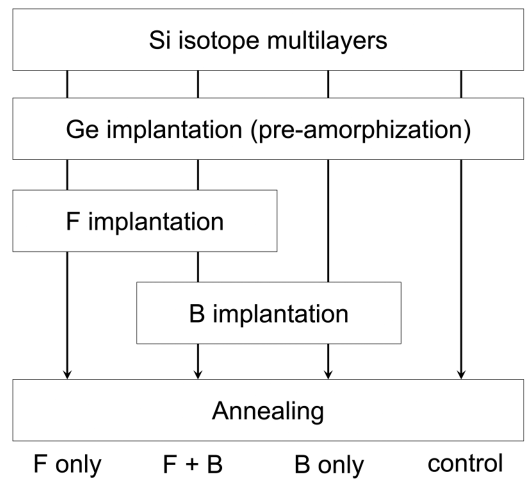

FIG. 1. A schematic flow chart of preparation of four groups of samples employed in this study.

III. RESULTS AND DISCUSSION

A. Effect of F on Si self- and B diffusion

Figure 2 shows the depth profiles of ^{30}Si, F, and B in F + B samples after Ge implantation (before annealing) together with the ^{30}Si profile before Ge implantation (as-grown). The periodic ^{30}Si profile was perturbed after Ge implantation, as shown in Fig. 2. The Ge depth profile is also presented. This perturbation of the profile is due to the Si displacement induced by Ge implantation.[29] The pre-amorphized regions of all the samples employed in this study should be fully recrystallized after annealing at 800–950 °C for 30 s–2 h because annealing temperatures used in this study are well above the temperature used to recrystallize F-implanted pre-amorphized Si and recrystallization takes place rather instantaneously.[8]

Figure 3(a) shows the depth profiles after annealing at 950 °C for 30 min. The diffusion of F and B in F + B samples and that in B only and F only samples are observed in the same annealing. The profiles after annealing can be directly compared because as-implanted profiles in these three types of samples are practically identical. As expected, the B profile in F + B samples shows the suppression of B diffusion, compared with that in B only samples. This clearly shows the effect of F on the suppression of B diffusion. In addition, Si self-diffusion is observed in all the Si isotope multilayers located between the surface and 450 nm in depth. In Fig. 3(b), the appreciable enhancement of Si self-diffusion at

Published under license by AIP Publishing.

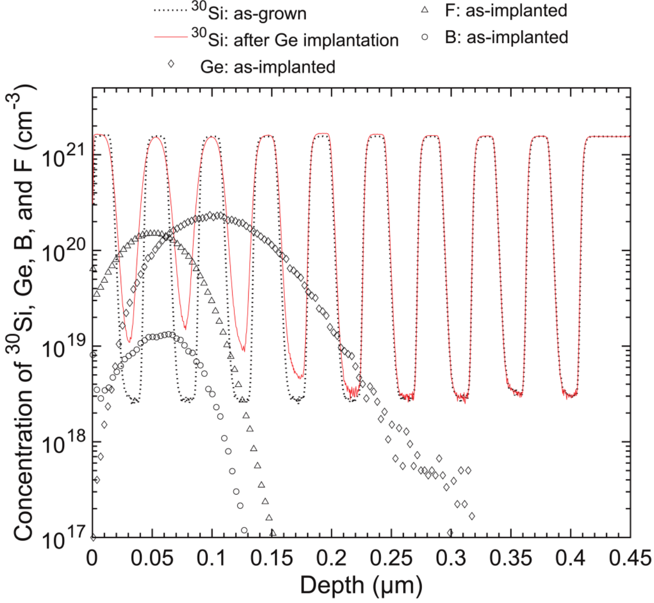

FIG. 2. SIMS profiles of ^{30}Si, Ge, F, and B in the F + B sample before annealing. The Si isotope multilayers were amorphized by Ge implantation prior to implantation by F and B. The solid line represents the profile of ^{30}Si in the ^{nat}Si/^{28}Si isotope multilayers after Ge implantation, and the dotted line represents the ^{30}Si profile before Ge implantation (as-grown). Open diamonds, triangles, and circles are the as-implanted profiles of Ge (150 keV, 2×10^{15} cm^{-2}), F (25 keV, 1×10^{15} cm^{-2}), and B (15 keV, 1×10^{14} cm^{-2}), respectively.

~200 nm in depth can be attributed to the effect of tensile strain induced by EOR defects, which are formed just beneath where the amorphous/crystalline interface existed, i.e., at the depth of 175–225 nm, as was observed in our previous study.[26] In order to investigate the effect of F on Si self-diffusion, the ratio of the time-averaged self-diffusivities in the sample with F (F only) to that without F (control) at the positions of each valley in the ^{30}Si profile of the isotope multilayers is obtained numerically as shown in Fig. 3(c). The ratio obtained indicates that Si self-diffusion is enhanced by the presence of F in the region shallower than where the EOR defects exist. Note that the largest enhancement of Si self-diffusion is observed in the second layer from the surface, where the F-implanted peak (~70 nm) is located. On the other hand, no significant enhancement by the presence of F is observed in the region deeper than where EOR defects exist (x > 175 nm). This can be ascribed to the contribution of EOR defects acting as a sink for V. The same trend of Si self-diffusion is observed in F + B samples.

Si self-diffusion occurs via interstitial and vacancy mechanisms.[23,24,30] Therefore, the enhanced Si self-diffusion observed in the present experiment indicates the increase in the concentration of either I or V. In addition, the suppression of B diffusion observed in F + B samples [Fig. 3(a)] indicates that the I concentration is reduced by the presence of F because B diffuses by the interstitial mechanism.[31] Therefore, the enhanced Si self-diffusion observed in the F-implanted region can be attributed to the

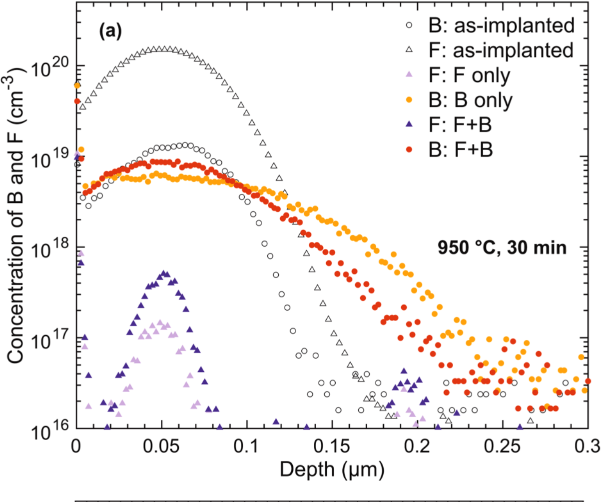

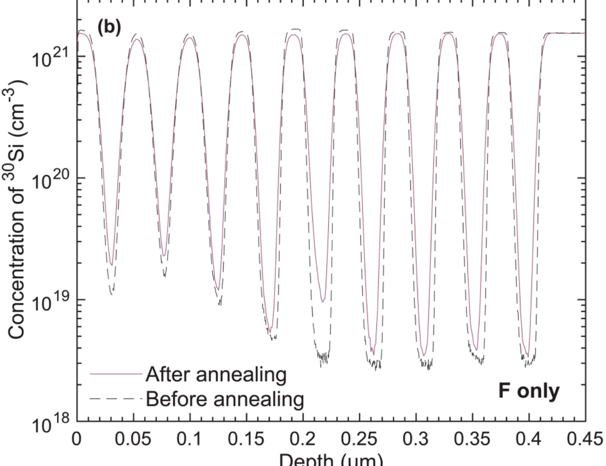

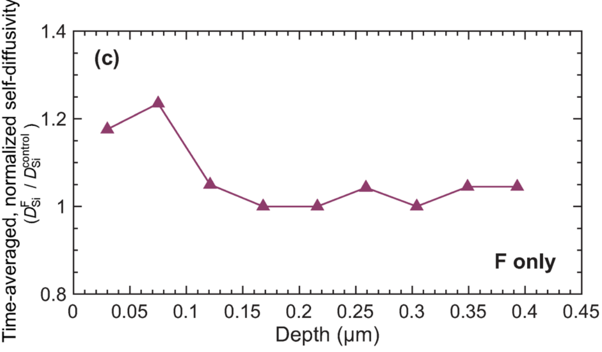

FIG. 3. (a) SIMS profiles of F and B after annealing at 950 °C for 30 min in F only, B only, and F + B samples. As-implanted profiles of F (open triangles) and B (open circles) that are practically identical for the three groups of samples are also shown. (b) SIMS profiles of ^{30}Si before (broken line) and after annealing at 950 °C for 30 min (solid line) in F only samples. (c) Ratio of the time-averaged Si self-diffusivities at 950 °C for 30 min in the sample with F (F only) to that without F (control) at the positions of each valley in the ^{30}Si profile of the isotope multilayers. The solid line is a guide to the eye.

Published under license by AIP Publishing.

increase of V concentration owing to the presence of F. In the past, the formation of FV clusters, such as F_3V, in F-implanted and annealed Si has been reported.[14–19,21] Indeed, the shape and the time-dependent behavior of F profiles observed in the present study strongly suggest the formation and dissolution of F-related clusters. In addition, the suppressed B diffusion by the presence of F has been explained by the I undersaturation owing to FV clusters.[9,11–13] Therefore, the enhanced Si self-diffusion observed in the present experiment can be explained by the increase in the concentration of V that are emitted upon the dissolution of FV clusters, while B diffusion is reduced by I undersaturation due to the increase in V concentration (V supersaturation).

Another noticeable feature of the results in Fig. 3(a) is that the peak concentration of F in F + B samples is about three times larger than that in F only samples after annealing. A similar trend is also seen in Fig. 4, where the depth profiles of F and B in F + B, F only, and B only samples after annealing at 900 °C for 30 min are shown. These results indicate that the dissolution of FV clusters was suppressed by the presence of B. In addition, not only the effect of B on F behaviors but also the effect of F on B diffusion in the B peak region is observed in Fig. 4. B atoms are found to be almost immobile around the B peak in F + B samples, whose region coincides with the peak of F. This characteristic pinning of B diffusion at around ∼50 nm in depth is so strong that it cannot be accounted for by the V emission from FV clusters. These results suggest that there is a direct interaction between F and B especially when F and B atoms coexist at high concentrations.[2,3,7] Therefore, the overall picture of suppression of B diffusion by F is that the direct F–B interaction plays the key role in the region of high F concentration ($>10^{17}\,cm^{-3}$), while the V emission from FV clusters becomes dominant in the low F concentration region.

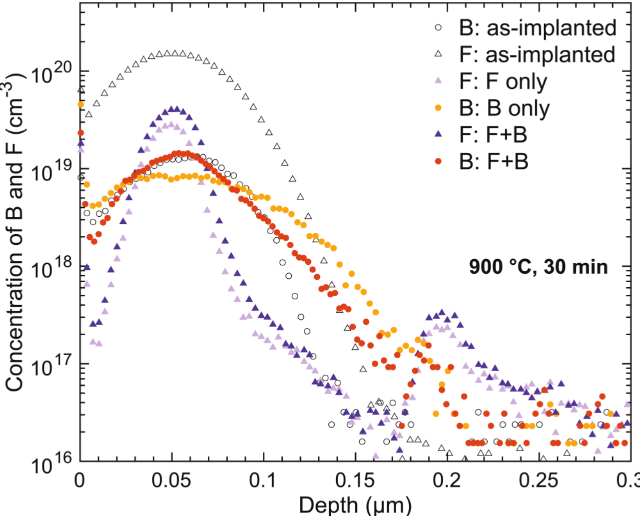

FIG. 4. SIMS profiles of F and B after annealing at 900 °C for 30 min in F only, B only, and F + B samples. The SIMS profiles before annealing (as-implanted) are also shown by open symbols.

Having established the importance of both F–B interaction and V originating from dissolution of FV clusters, let us analyze why previous experimental results were able to be modeled by taking into account only one of the two mechanisms. In Ref. 7, it was shown that F did not affect the diffusion of a buried B layer, which was located away from the F region; F were placed in the region shallower than the EOR defect region, while the buried B layer was placed deeper than where the EOR defects were.[7] Our results of Si self-diffusion using isotope multilayers shown in Fig. 2(c) reveal that the presence of F in the region shallower than EOR defects does not change significantly the I concentration in the deeper region. Therefore, our finding that B diffusion being suppressed by both the V emission and the F–B interaction agrees with the experimental results of Ref. 7. No direct F–B interaction was observed in the experiment performed in Ref. 12, but as the present experiment shows, the direct F–B interaction occurs only when F and B atoms coexist at high concentrations; the concentrations of F and B in Ref. 12 were only about 1/10 and 1/2 of those in ours, respectively.

Summarizing this section, Si self-, F, and B diffusions are simultaneously observed using Si isotope multilayers that are co-implanted with F and B. We have shown that B diffusion is suppressed by both the direct F–B interaction and the I undersaturation caused by dissolution of FV clusters.

B. Modeling of V emission upon FV cluster dissolution

Figures 5(a) and 5(b) show the F profiles in F only samples after annealing at 800 and 950 °C, respectively. It is seen that, even without a capping layer on the top, out-diffusion of F to the surface is rather limited. Similar to the F profiles shown in Figs. 3(a) and 4, notable features of the F behaviors are (i) substantial dose loss and (ii) non-Fickian diffusion profiles. These characteristics were observed in all the annealing conditions employed in the study. The dose loss of F is attributed to the combination of fast diffusion and continuous evaporation of F from the surface during the thermal treatment.[32,33] The retained F dose decreases with the annealing time but the shape of the F profile does not broaden. Such a characteristic behavior suggests that F impurities are forming clusters such as FV for there is supersaturation of V as described in Sec. III A. FV clusters are formed to retain the F dose in the very early stage of annealing, that is, during the solid-phase epitaxial regrowth of the amorphous region.[12,34] The decrease is due to the dissolution of FV clusters, and F atoms that are released diffuse out to the surface to evaporate.

A closer look at the change of F profiles with time reveals that the dissolution rate of the FV clusters decreases with the annealing time. In Fig. 5(a), the dissolution rate of FV clusters obtained from the F profile for 30 min annealing is larger than that obtained for 2 h annealing. The same trend holds for Fig. 5(b). Such time dependence of the dissolution rate of FV clusters implies that the FV clusters are stabilized by annealing.

In order to construct a model to fit our experimental F diffusion profiles, we first consider the formation and dissolution of FV clusters. According to first-principles calculations, the dominant configurations of FV clusters are F_3V and F_6V_2, the latter being more stable.[14] The contribution of F_3V and F_6V_2 is also supported

Published under license by AIP Publishing.

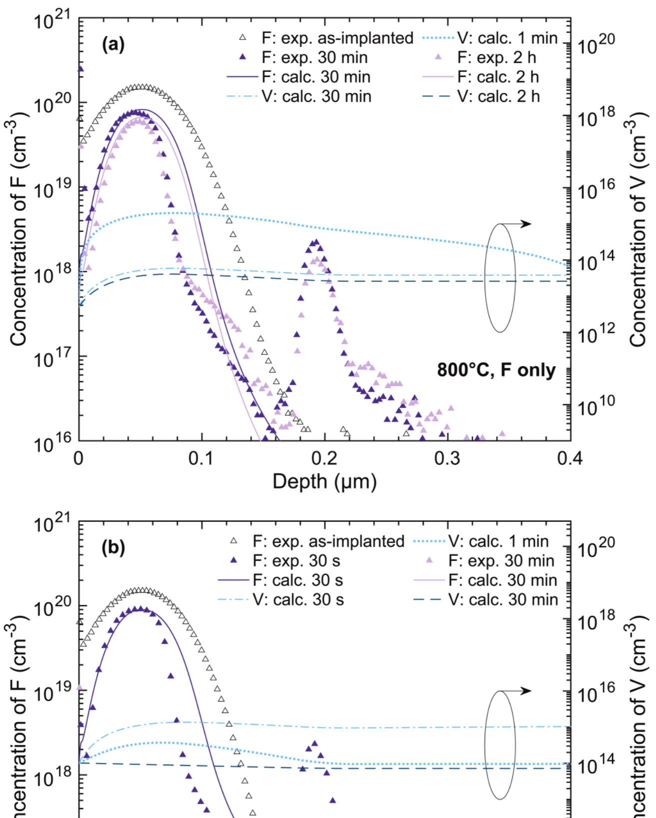

FIG. 5. SIMS and simulated profiles of F in F only samples after annealing (a) at 800 °C for 30 min and 2 h and (b) at 950 °C for 30 s and 30 min. The as-implanted profile of F (before annealing) is also shown. Symbols and solid lines represent SIMS and simulated profiles, respectively. In addition, the depth profiles of V deduced from the simulation, together with those for 1 min, are shown.

by the analysis based on positron annihilation spectroscopy and SIMS.[18] These results let us assume a rapid formation of F_3V in the very early stage of annealing during the regrowth process of the amorphized layer and a configuration change from F_3V to F_6V_2 during annealing, where F_6V_2 is more stable having a smaller dissolution rate. Among various possible structures, our model takes into account the most stable F_3V and F_6V_2 clusters to simplify the model calculation.

Our model of FV clusters consists of the following four reactions:

(i) Formation of F_3V: three F interstitial atoms (F_i) form one F_3V cluster during the regrowth of the amorphized layer.

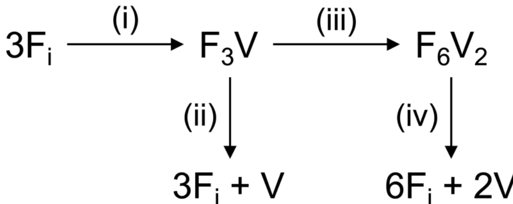

FIG. 6. A reaction pathway for the formation and dissolution of FV clusters in our model. Reaction (iii) means formation of one F_6V_2 cluster from two F_3V clusters.

(ii) Dissolution of F_3V: three F_i and one V are emitted (released) upon dissolution of one F_3V cluster. F_i out-diffuse to evaporate from the surface.

(iii) Formation of F_6V_2: two F_3V clusters form one F_6V_2 cluster.

(iv) Dissolution of F_6V_2: six F_i and two V are emitted upon the dissolution of one F_6V_2 cluster. F_i out-diffuse to evaporate from the surface.

The reaction pathway is shown in Fig. 6. These reactions lead to the following set of coupled partial differential equations:

$$\frac{\partial C_{F_i}}{\partial t} = \frac{\partial}{\partial x}\left(D_{F_i}\frac{\partial C_{F_i}}{\partial x}\right) - 3G^f_{F_3V} + 3G^d_{F_3V} + 6G^d_{F_6V_2}, \tag{1}$$

$$\frac{\partial C_{F_3V}}{\partial t} = G^f_{F_3V} - G^d_{F_3V} - 2G^f_{F_6V_2}, \tag{2}$$

$$\frac{\partial C_{F_6V_2}}{\partial t} = G^f_{F_6V_2} - G^d_{F_6V_2}, \tag{3}$$

$$\frac{\partial C_I}{\partial t} = \frac{\partial}{\partial x}\left(D_I\frac{\partial C_I}{\partial x}\right) - G_{311} - G_{EOR} - G_{TypeIII} + G_{Re}, \tag{4}$$

$$\frac{\partial C_V}{\partial t} = \frac{\partial}{\partial x}\left(D_V\frac{\partial C_V}{\partial x}\right) + G^d_{F_3V} + 2G^d_{F_6V_2} + G_{Re}, \tag{5}$$

where D_X is the diffusivity of X [X = F_i, I, V], C_X is the concentration of X [X = F_i, F_3V, F_6V_2, I, V], and G^f_X and G^d_X are the terms of formation and dissolution of X [X = F_3V, F_6V_2], respectively,

$$G^f_{F_3V} = k^f_{F_3V} C^3_{F_i}, \tag{6}$$

$$G^d_{F_3V} = k^d_{F_3V} C_{F_3V} \frac{C^{FF}_{F_3V}}{(C_{F_3V} + C^{FF}_{F_3V})}, \tag{7}$$

$$G^f_{F_6V_2} = k^f_{F_6V_2} C^2_{F_3V}, \tag{8}$$

$$G^d_{F_6V_2} = k^d_{F_6V_2} C_{F_6V_2} \frac{C^{FF}_{F_6V_2}}{(C_{F_6V_2} + C^{FF}_{F_6V_2})}, \tag{9}$$

Published under license by AIP Publishing.

where Eqs. (6)–(9) denote reactions (i), (ii), (iii), and (iv) in Fig. 6, respectively.

G_{Re} is the generation term for I–V generation–recombination (g–r) described by the following reaction:

$$G_{Re} = k_{Re}(C_I^{eq}C_V^{eq} - C_I C_V), \tag{10}$$

where k_{Re} is the g–r rate, and C_I^{eq} and C_V^{eq} represent the equilibrium concentrations of I and V, respectively. In order to describe I emission from the implantation-induced defects, we use the diffusion model involving the time evolution of {311} clusters (G_{311}) and that of EOR defects (G_{EOR}) that has been used in our previous study.[26] In addition, the effect of type III defects[35] formed upon the regrowth of the amorphized layer ($G_{TypeIII}$) is taken into account in the same way as in the previous study.[36] In reaction (i) and Eq. (6), the contribution of V is not included, because the supply of V from the surface is negligibly small compared to that of F_i out-diffusion. It is supposed that V are supplied from the pre-amorphized layer during the regrowth process to form F_3V.

In Eqs. (6)–(9), k_X^f and k_X^d are the formation and the dissolution rate constants of X, respectively. C_X^{FF}, in which the superscript of FF stands for the effect of F on FV clusters, represents the characteristic concentration of X that determines the degree of reduction of the reaction parameter k_X^d with C_X. In Eq. (7), the dissolution rate of F_3V decreases in proportion to the concentration of F_3V, when the concentration of F_3V is higher than $C_{F_3V}^{FF}$, and the same for F_6V_2 in Eq. (9). This characteristic concentration is introduced to reproduce the distinctive F profiles, whose dose decreases with time while keeping its overall shape. The diffusivity of F_i, $D_{F_i} = 10^{-9}$ cm^2 s^{-1}, was set high enough to reproduce the dose loss of F. In order to simulate the evaporation of F from the surface, the out-diffusion flux is assumed to be proportional to C_{F_i}. The equilibrium concentrations of I and V are used at the Si surface. The contributions of I and V to Si self-diffusion are taken into account in the same way as in our previous study.[26] Using all the models mentioned above, diffusion equations are solved numerically by the partial differential equation solver ZOMBIE.[37]

Solid lines in Figs. 5(a) and 5(b) show the calculated profiles of F after annealing at 800 °C (for 30 min and 2 h) and 950 °C (for 30 s and 30 min), respectively. Here, the F profiles are obtained from the sum of the calculated results of C_{F_i}, $3 \times C_{F_3V}$, and $6 \times C_{F_6V_2}$. The calculation reproduces very well the SIMS profiles in Figs. 5(a) and 5(b). The F profiles in F only samples observed in the other experimental conditions can also be fitted. In addition, the simulated result of ^{30}Si in F only samples after annealing at 950 °C for 30 min reproduces well the SIMS profile, as shown in Fig. 7. The values of parameters in Eqs. (6)–(9) are determined in this study from the fitting of these profiles. Figure 8 shows some of these values in the Arrhenius format yielding $k_{F_3V}^d = 6.17 \times 10^9 \exp\left(-\frac{2.63\,\text{eV}}{k_B T}\right)$ s^{-1}, $k_{F_6V_2}^f = 8.81 \times 10^{-10} \exp\left(-\frac{2.77\,\text{eV}}{k_B T}\right)$ cm^3 s^{-1}, and $k_{F_6V_2}^d = 1.34 \times 10^9 \exp\left(-\frac{2.78\,\text{eV}}{k_B T}\right)$ s^{-1} from the fitting to the data. For the other parameters, the best fitting is obtained when temperature-independent values of $k_{F_3V}^f = 1.0 \times 10^{-37}$ cm^6 s^{-1}, $C_{F_3V}^{FF} = 3.0 \times 10^{19}$ cm^{-3}, and $C_{F_6V_2}^{FF} = 8.0 \times 10^{18}$ cm^{-3} are used.

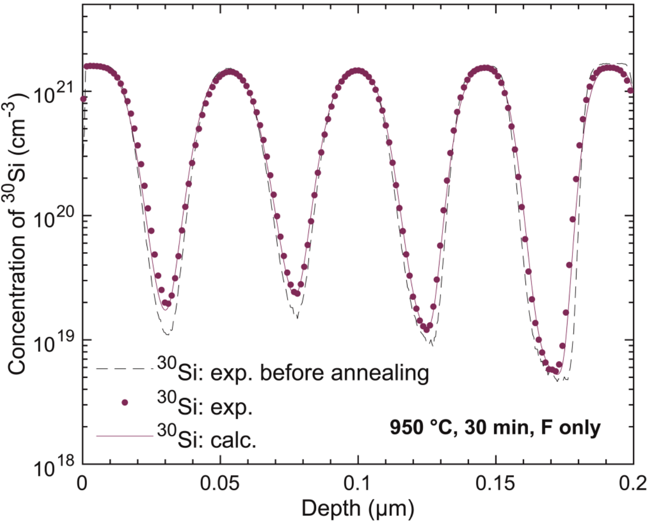

FIG. 7. SIMS and simulated profiles of ^{30}Si in F only samples after annealing at 950 °C for 30 min. Filled circles and solid lines represent SIMS and simulated profiles, respectively. The SIMS profile before annealing is also shown by a dashed line.

The obtained value of $k_{F_6V_2}^d$ is about one order of magnitude smaller than that of $k_{F_3V}^d$, which is consistent with the assumption that F_6V_2 is more stable than F_3V. $C_{F_6V_2}^{FF}$ is smaller than $C_{F_3V}^{FF}$ showing that the effect of F_6V_2 on the suppression of the dissolution rate at the high concentration region is more pronounced than that of F_3V. This suggests that the larger cluster, F_6V_2, interacts more strongly with neighbors than the smaller F_3V.

The depth profiles of V deduced from the simulation during annealing at 800 °C (950 °C) for 1 min, 30 min, and 2 h (30 s, 1

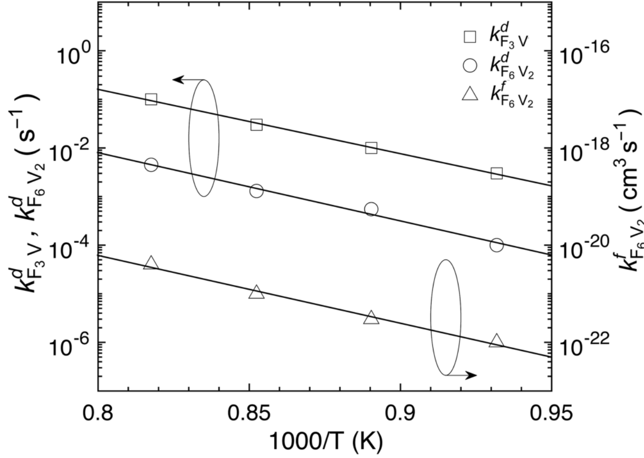

FIG. 8. Temperature dependence of the reaction rate constants deduced from the calculation for $k_{F_3V}^d$ (open squares), $k_{F_6V_2}^d$ (open circles), and $k_{F_6V_2}^f$ (open triangles). The solid lines represent Arrhenius fittings to the data.

Published under license by AIP Publishing.

min, and 30 min) are shown in Fig. 5(a) [Fig. 5(b)]. For the equilibrium concentration of V, we use the values from Ref. 23. The concentration profiles of V show the supersaturation of V, especially in the region shallower than the region of the EOR defects, which act as a sink for V. At 950 °C for 30 min, when only a small amount of FV clusters to emit V remains, the V concentration approaches its equilibrium value throughout the investigated region. Note that the concentration profile of V at 950 °C for 1 min shows the supersaturation of V at ~70 nm in depth, where the F-implanted peak is located. This profile is consistent with the time-averaged and normalized Si self-diffusivity in Fig. 3(c), which shows the largest enhancement of Si self-diffusion in the second layer from the surface, while no significant enhancement occurs in the region deeper than the EOR defect region.

In Figs. 3(a), 4, and 5, the F profiles exhibit a peak at a depth of ~200 nm indicating F trapping by EOR defects. Such trapping was observed in the previous study.[38] However, the present study does not model such trapping because trapped F do not affect diffusion of B. Similar trapping of carbon (C) by EOR defects was observed in C-implanted and annealed Si, and, in this case, Si self-diffusion was enhanced.[27] In contrast, in the present case, simulation of Si self-diffusion is possible without including the effect of F being trapped at EOR defects (Fig. 7). In addition, the stability of EOR defects do not change by the trapping of low concentration of F.[10] Although it can be modeled in a similar way as was done for C trapping,[27] additional model for this F trapping by EOR defects is not taken into account in the present simulation, since our purpose is to model the effect of F on the suppression of B diffusion.

C. Simulation of B diffusion suppressed by F

Simulation of B diffusion suppressed by the presence of F is performed by adding the B diffusion model in the same way as in the previous study.[25] The formation of BI clusters is not taken into account because BI clustering is unlikely in the pre-amorphized Si. The simulation of B diffusion reproduces very well the experimentally obtained B profiles in B only samples for all the annealing conditions employed in this study.

As described in Sec. III A, the suppression of B diffusion by the presence of F is attributed to both the V supersaturation induced by FV clusters and direct F–B interaction. Our simulation takes into account the V emission from FV clusters, as described in Sec. III B, but neglects F–B interaction at this point. In order to investigate the effect of F–B interaction, we first fit the profiles of B and F by using the simulation that does not take F–B interaction into account. Figure 9 shows the SIMS profiles of B and F in F + B samples after annealing in various conditions: (a) 950 °C for 30 min, (b) 950 °C for 30 s, (c) 900 °C for 30 min, (d) 850 °C for 1 h, and (e) 800 °C for 2 h. The SIMS profiles in Figs. 9(a) and 9(c) are from those in Figs. 3(a) and 4, respectively. Broken lines in Fig. 9 show the calculated profiles of B without F-B interaction (as indicated by "No F-B" in the figure), which clearly overestimate the experimental B diffusion, especially at higher temperatures of 900 and 950 °C. For comparison, dotted lines in Fig. 9 represent the calculated B profiles without V emission from FV clusters or F–B interaction ("No FVcl or F-B"), which, as expected, fit only the B profiles in B only samples. These comparisons clearly show the suppression by the V supersaturation, that is, I undersaturation induced by FV clusters. Such suppression by the V emission alone, however, cannot satisfactorily account for the suppression of B diffusion around the B peak, where B atoms are almost immobile. Figure 9 also shows the calculated profiles of F without F–B interaction ("No F-B"), which certainly fit the experimental F profiles in F only samples, but overestimate the decrease of the F concentration. Let us mention here that two separated F peaks due to FV clusters and F–B interaction would have been observed if the F and B profiles were spatially separated. Such an observation was reported in the previous study.[38] In our work, the peak of F profile situates close to that of B, and, therefore, the two F peaks from FV clusters and F–B interaction overlap.

In order to complete the model, we include the F–B interaction to improve the simulation for the region that contains high concentrations of B and F. The retardation factors are introduced into B diffusion and the dissolution of FV clusters as follows:

$$D'_{\mathrm{B_i}} = D_{\mathrm{B_i}} \times \frac{C^{\mathrm{FB}}_{\mathrm{F_3V}}}{C_{\mathrm{F_3V}} + C^{\mathrm{FB}}_{\mathrm{F_3V}}} \times \frac{C^{\mathrm{FB}}_{\mathrm{F_6V_2}}}{C_{\mathrm{F_6V_2}} + C^{\mathrm{FB}}_{\mathrm{F_6V_2}}}, \tag{11}$$

$$K^d_{\mathrm{F_3V}} = k^d_{\mathrm{F_3V}} \times \frac{C^{\mathrm{BF1}}_{\mathrm{B}}}{C_{\mathrm{B}} + C^{\mathrm{BF1}}_{\mathrm{B}}}, \tag{12}$$

$$K^d_{\mathrm{F_6V_2}} = k^d_{\mathrm{F_6V_2}} \times \frac{C^{\mathrm{BF2}}_{\mathrm{B}}}{C_{\mathrm{B}} + C^{\mathrm{BF2}}_{\mathrm{B}}}, \tag{13}$$

where $D'_{\mathrm{B_i}}$ is the retarded diffusivity of B interstitials ($\mathrm{B_i}$), which is substituted for $D_{\mathrm{B_i}}$ in the B diffusion equation [see Eq. (8) in Ref. 25]. $K^d_{\mathrm{F_3V}}$ and $K^d_{\mathrm{F_6V_2}}$ are the suppressed dissolution rates of FV clusters, which are substituted for $k^d_{\mathrm{F_3V}}$ and $k^d_{\mathrm{F_6V_2}}$ in Eqs. (7) and (9), respectively. In Eqs. (11)–(13), the superscript FB stands for the effect of F on B diffusion, and BF1 and BF2 for that of B on $\mathrm{F_3V}$ and $\mathrm{F_6V_2}$, respectively. The retardation effects are modeled in the same manner as in Eqs. (7) and (9), where Eq. (11) indicates the retardation of B diffusion as a function of $C_{\mathrm{F_3V}}$ and $C_{\mathrm{F_6V_2}}$, and Eqs. (12) and (13) represent that of the dissolution of $\mathrm{F_3V}$ and $\mathrm{F_6V_2}$ as a function of B concentration (C_{B}), respectively. In Eq. (11), the B diffusivity decreases proportionally to $C_{\mathrm{F_3V}}$, when $C_{\mathrm{F_3V}}$ is higher than $C^{\mathrm{FB}}_{\mathrm{F_3V}}$, and the same holds for $\mathrm{F_6V_2}$. In Eq. (12), the dissolution rate of $\mathrm{F_3V}$ decreases proportionally to C_{B}, when C_{B} is higher than $C^{\mathrm{BF1}}_{\mathrm{B}}$, and the same for $\mathrm{F_6V_2}$ in Eq. (13). Equations (11)–(13) are added to the simulation used above, and the characteristic concentrations $C^{\mathrm{FB}}_{\mathrm{F_3V}}$, $C^{\mathrm{FB}}_{\mathrm{F_6V_2}}$, $C^{\mathrm{BF1}}_{\mathrm{B}}$, and $C^{\mathrm{BF2}}_{\mathrm{B}}$ are the fitting parameters in the simulation. The solid lines denoted by "FVcl + F-B" in Fig. 9 represent the simulated B and F profiles after the annealing. The calculated results reproduce very well the SIMS profiles in F + B samples observed in the entire experimental conditions. The best fitting is obtained when temperature-independent values of $C^{\mathrm{FB}}_{\mathrm{F_3V}} = 4.0 \times 10^{19}\ \mathrm{cm^{-3}}$, $C^{\mathrm{FB}}_{\mathrm{F_6V_2}} = 1.0 \times 10^{17}\ \mathrm{cm^{-3}}$, $C^{\mathrm{BF1}}_{\mathrm{B}} = 7.0 \times 10^{19}\ \mathrm{cm^{-3}}$, and $C^{\mathrm{BF2}}_{\mathrm{B}} = 7.0 \times 10^{19}\ \mathrm{cm^{-3}}$ are selected. Our model reproduces important features of experimental profiles in the literature, e.g., the decrease of F dose while keeping its overall shape[1] and the increase of F concentration when F and B coexist.[39] In the previous models,[20–22] the effect of FV clusters was

Published under license by AIP Publishing.

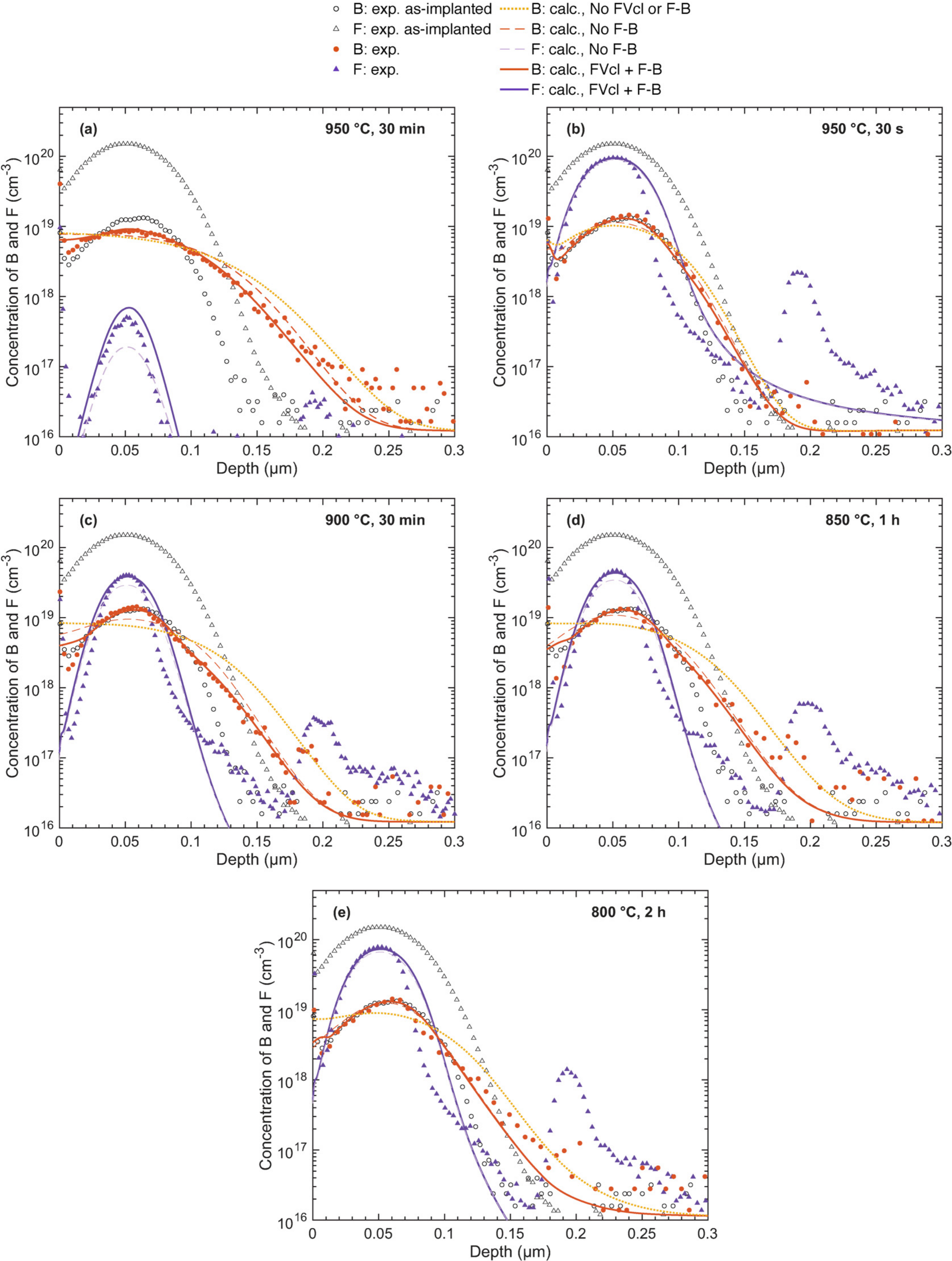

FIG. 9. SIMS and simulated profiles of F and B in F + B samples after annealing: (a) 950 °C for 30 min, (b) 950 °C for 30 s, (c) 900 °C for 30 min, (d) 850 °C for 1 h, and (e) 800 °C for 2 h. The as-implanted profiles of B and F (before annealing) are also shown. Filled symbols represent SIMS profiles. Solid lines represent the simulated profiles of F and B based on our model that takes into account the V emission from FV clusters and F–B interaction (FVcl + F-B). Light purple dashed lines are the calculated results of F without F–B interaction (No F-B), and orange dashed and dotted lines are those of B without F–B interaction (No F-B) and without V emission from FV clusters nor F–B interaction (No FVcl or F-B). FVcl and F-B stand for V emission from FV clusters and F–B interaction, respectively.

Published under license by AIP Publishing.

taken into account while that of F–B interaction was not. Such models would work well for the prediction of B diffusion when F and B concentration peaks were spatially separated. In the case of the overlapping F and B peaks, the previous models fail to predict the immobile B profiles at the F peak region. The model for the overlapping F and B profiles is needed to model BF_2 implantation that is widely employed in the industry.

It was suggested that F atoms were to form chemical bonding with B atoms to retard B diffusion.[7] In our experiments, the retardation of B diffusion is quite striking at the F peak region for the annealing at 950 °C for 30 s [Fig. 9(b)] but becomes much less for 30 min [Fig. 9(a)]. Such time dependence suggests that F–B interaction to retard B diffusion is less of the chemical bonding type. Here, the F–B interaction we consider is trapping of B atoms by FV clusters. Due to the F–B interaction, diffusing B are attracted and trapped by F that form FV clusters. Because of this trapping, the F–B interaction leads to the reduction in B diffusion. In the simulation, the value of $C^{FB}_{F_6V_2}$ is found to be smaller than that of $C^{FB}_{F_3V}$, indicating that B trapping by F_6V_2 is stronger than that by F_3V, consistent with the already mentioned trend that F_6V_2 interacts more strongly with the clusters in the neighborhood than F_3V. In contrast, no apparent difference is obtained between the value of C^{BF1}_{B} for F_3V and that of C^{BF2}_{B} for F_6V_2; suppression of the cluster dissolution by trapped B does not depend significantly on the size of FV clusters. Not the strength of the interaction between B and FV clusters but the release of B atoms from the trapping upon the dissolution of FV clusters determines the characteristic concentration of C^{BF1}_{B} and C^{BF2}_{B}.

Finally, let us point out that the concentration of Ge used for pre-amorphization is very small, much less than 0.5% of the matrix silicon, and the presence of Ge does not affect the diffusion of B, Si, and F as can be seen in Fig. 2. Here, the Ge peak (depth ~100 nm) is shifted from that of F and B (depth ~50 nm) and a steep gradient in the Ge concentration exists in the pre-amorphized region (Fig. 2). However, even with this rapid background spatial change in Ge density, the diffusion profiles of B and Si can be modeled quantitatively very well by the well-known models of B and self-diffusion in pure Si. The diffusion of F in this region can also be modeled well assuming a pure silicon matrix without the effect of background Ge.

IV. CONCLUSIONS

We have simultaneously observed Si self-, B, and F diffusion using pre-amorphized $^{nat}Si/^{28}Si$ isotope multilayers that are co-implanted with B and F. The behaviors of I and V are directly observed through ^{30}Si diffusion. Because of the presence of F, Si self-diffusion is enhanced in the region shallower than the region of EOR defects due to the increase in the concentration of V that is emitted upon the dissolution of FV clusters. Moreover, the B and F profiles show that B diffusion is reduced at the F peak region, where B atoms are almost immobile, and that the dissolution of FV clusters is suppressed by the presence of B, which suggests a direct interaction between F and B. These results lead us to conclude that B diffusion is retarded by both the V supersaturation caused by FV clusters and the direct F–B interaction.

From such experimental results, we established models for the formation and dissolution of FV clusters and for the F–B interaction. The effects of F_3V and F_6V_2 clusters are included to describe the decrease in the dissolution rates with annealing time. In addition, the characteristic concentration, above which the dissolution rate of FV clusters decreases, is introduced to reproduce the distinctive experimental profiles of F. F atoms released upon the dissolution of FV clusters out-diffuse to evaporate from the surface during the annealing, resulting in a significant loss of the dose of F. F–B interaction is also included to account for the retardation of B diffusion and suppression of dissolution of FV clusters when F and B atoms coexist at high concentrations. The diffusion calculation based on the model developed in this study agrees with the experimental profiles taken under various sample and annealing conditions. Therefore, the present model is directly applicable in the process simulation of B and F behaviors for the production of Si transistors.

ACKNOWLEDGMENTS

We acknowledge Yasuo Shimizu for fruitful discussions. This work was supported in part by Grants-in-Aid for Scientific Research from the Japan Society for the Promotion of Science (No. 17K06397).

DATA AVAILABILITY

The data that support the findings of this study are available from the corresponding author upon reasonable request.

REFERENCES

[1] A. J. Walker, J. Appl. Phys. **71**, 2033 (1992).
[2] L. Y. Krasnobaev, N. M. Omelyanovskaya, and V. V. Makarov, J. Appl. Phys. **74**, 6020 (1993).
[3] J. Liu, D. F. Downey, K. S. Jones, and E. Ishida in *Proceedings of International Conference on Ion Implantation Technology, Kyoto, Japan* (IEEE, 1998), p. 951.
[4] D. F. Downey, J. W. Chow, E. Ishida, and K. S. Jones, Appl. Phys. Lett. **73**, 1263 (1998).
[5] T. Shano, R. Kim, T. Hirose, Y. Furuta, H. Tsuji, M. Furuhashi, and K. Taniguchi, in *International Electron Devices Meeting. Technical Digest* (IEEE, 2001), p. 37.4.1.
[6] S. C. Jain, W. Schoenmaker, R. Lindsay, P. A. Stolk, S. Decoutere, M. Willander, and H. E. Maes, J. Appl. Phys. **91**, 8919 (2002).
[7] A. Mokhberi, R. Kasnavi, P. B. Griffin, and J. D. Plummer, Appl. Phys. Lett. **80**, 3530 (2002).
[8] G. Impellizzeri, J. H. R. dos Santos, S. Mirabella, F. Priolo, E. Napolitani, and A. Carnera, Appl. Phys. Lett. **84**, 1862 (2004).
[9] H. A. W. El Mubarek, J. M. Bonar, G. D. Dilliway, P. Ashburn, M. Karunaratne, A. F. Willoughby, Y. Wang, P. L. F. Hemment, R. Price, J. Zhang, and P. Ward, J. Appl. Phys. **96**, 4114 (2004).
[10] N. E. B. Cowern, B. Colombeau, J. Benson, A. J. Smith, W. Lerch, S. Paul, T. Graf, F. Cristiano, X. Hebras, and D. Bolze, Appl. Phys. Lett. **86**, 101905 (2005).
[11] M. N. Kham, H. A. W. El Mubarek, J. M. Bonar, and P. Ashburn, Appl. Phys. Lett. **87**, 011902 (2005).
[12] G. Impellizzeri, S. Mirabella, F. Priolo, E. Napolitani, and A. Carnera, J. Appl. Phys. **99**, 103510 (2006).
[13] M. N. Kham, I. Matko, B. Chenevier, and P. Ashburn, J. Appl. Phys. **102**, 113718 (2007).
[14] M. Diebel and S. T. Dunham, Phys. Rev. Lett. **93**, 245901 (2004).

Published under license by AIP Publishing.

[15]G. M. Lopez, V. Fiorentini, G. Impellizzeri, S. Mirabella, and E. Napolitani, Phys. Rev. B **72**, 045219 (2005).
[16]X. D. Pi, C. P. Burrows, and P. G. Coleman, Phys. Rev. Lett. **90**, 155901 (2003).
[17]P. J. Simpson, Z. Jenei, P. Asoka-Kumar, R. R. Robison, and M. E. Law, Appl. Phys. Lett. **85**, 1538 (2004).
[18]D. A. Abdulmalik, P. G. Coleman, N. E. B. Cowern, A. J. Smith, B. J. Sealy, W. Lerch, S. Paul, and F. Cristiano, Appl. Phys. Lett. **89**, 052114 (2006).
[19]T. Umeda, J. Isoya, T. Ohiyama, S. Onoda, N. Morishita, K. Okonogi, and S. Shiratake, Appl. Phys. Lett. **97**, 041911 (2010).
[20]E. M. Bazizi, K. R. C. Mok, F. Benistant, S. H. Yeong, R. S. Teo, and C. Zechner, AIP Conf. Proc. **1496**, 249 (2012).
[21]R. Robison and M. E. Law, in *Technical Digest. International Electron Devices Meeting* (IEEE, 2002), p. 883.
[22]F. A. Wolf, A. Martinez-Limia, and P. Pichler, Solid State Electron. **87**, 4 (2013).
[23]H. Bracht, H. H. Silvestri, I. D. Sharp, and E. E. Haller, Phys. Rev. B **75**, 035211 (2007).
[24]Y. Shimizu, M. Uematsu, and K. M. Itoh, Phys. Rev. Lett. **98**, 095901 (2007).
[25]Y. Shimizu, M. Uematsu, K. M. Itoh, A. Takano, K. Sawano, and Y. Shiraki, J. Appl. Phys. **105**, 013504 (2009).
[26]T. Isoda, M. Uematsu, and K. M. Itoh, J. Appl. Phys. **118**, 115706 (2015).
[27]T. Isoda, M. Uematsu, and K. M. Itoh, Jpn. J. Appl. Phys. **55**, 036504 (2016).
[28]T. Kojima, R. Nebashi, K. M. Itoh, and Y. Shiraki, Appl. Phys. Lett. **83**, 2318 (2003).
[29]Y. Shimizu, M. Uematsu, K. M. Itoh, A. Takano, K. Sawano, and Y. Shiraki, Appl. Phys. Express **1**, 021401 (2008).
[30]T. Südkamp and H. Bracht, Phys. Rev. B **94**, 125208 (2016).
[31]H.-J. Gossmann, T. E. Haynes, P. A. Stolk, D. C. Jacobson, G. H. Gilmer, J. M. Poate, H. S. Luftman, T. K. Mogi, and M. O. Thompson, Appl. Phys. Lett. **71**, 3862 (1997).
[32]S. P. Jeng, T. P. Ma, R. Canteri, M. Anderle, and G. W. Rubloff, Appl. Phys. Lett. **61**, 1310 (1992).
[33]C. Szeles, B. Nielsen, P. Asoka-Kumar, K. G. Lynn, M. Anderle, T. P. Ma, and G. W. Rubloff, J. Appl. Phys. **76**, 3403 (1994).
[34]M. Diebel, S. Chakravarthi, S. T. Dunham, C. F. Machala, S. Ekbote, and A. Jain, Mater. Res. Soc. Symp. Proc. **765**, D6.15.1 (2003).
[35]K. S. Jones, S. Prussin, and E. R. Weber, Appl. Phys. A **45**, 1 (1988).
[36]M. Uematsu, Jpn. J. Appl. Phys. **37**, 5866 (1998).
[37]W. Jüngling, P. Pichler, S. Selberherr, E. Guerrero, and H. W. Pötzl, IEEE Trans. Electron Devices **32**, 156 (1985).
[38]N. Ohno, T. Hara, Y. Matsunaga, and M. I. Current, Ion Implant. Tech. Proc. **2**, 1047 (1998).
[39]G. Impellizzeri, S. Mirabella, E. Bruno, F. Priolo, E. Napolitani, and A. Carnera, J. Vac. Sci. Technol. B **24**, 433 (2006).

Published under license by AIP Publishing.